A Comparative Assessment of Calibrated SDRs for Spectrum Sensing

Parker Trzebunia PKTRZEBU@NCSU.EDU
North Carolina State University, 890 Oval Dr, Raleigh, NC 27606 USA

Wahab Khawaja WKHAWAJ@NCSU.EDU
North Carolina State University, 890 Oval Dr, Raleigh, NC 27606 USA

Ali Gurbuz ALIGURBUZ@NCSU.EDU
North Carolina State University, 890 Oval Dr, Raleigh, NC 27606 USA

Abstract

Cost-effective, reliable spectrum sensing systems are increasingly important in modern wireless systems. This paper presents the design and implementation of a spectrum sensing and detection system to compare the performance of five commercial software-defined radios (SDRs). The system scans and stitches subbands, normalizes the frequency response of the receiver, and returns a per-bin, threshold-based detection decision. terminated-input false-detection counts, settling interval, and scan/processing time are compared while considering receiver characteristics such as cost, frequency range, and maximum sampling rate. The SDRs are tested using controlled over-the-air signals and scans in the 902–928 MHz ISM band at 2.4 MS/s and 10 MS/s, and in the 2402–2480 MHz Bluetooth channel range at 10 MS/s, as their datasheet specifications allow.

1. Introduction

Spectrum sensing provides a receiver with evidence of activity within a frequency interval and supports dynamic spectrum access, interference monitoring, and radio-environment awareness (Yücek & Arslan, 2009), as well as RF-based detection of unmanned aerial vehicles (UAVs) (Chiper et al., 2022; Khan et al., 2022). Common approaches include energy detection, matched filtering, cyclostationary detection, and covariance-based methods (Yücek & Arslan, 2009). Energy detection is particularly attractive for a heterogeneous monitoring platform because it does not require prior knowledge of a signal's modulation, framing, or waveform (Urkowitz, 1967; Yücek & Arslan, 2009). However, applying the same software detector does not make measurements from different receivers directly comparable. Analog filtering, quantization, gain, frequency response, host transport, and retuning behavior influence the samples available to the detector. In addition, uncertainty in the noise power used to set a detection threshold can limit energy-detection performance (Tandra & Sahai, 2008; Mariani et al., 2011). These considerations motivate a comparison that combines receiver calibration with measurements of false alarms and scan time.

The study evaluates five commercially available receivers:

- RTL-SDR Blog V3;
- Nooelec NESDR SMArt XTR;
- Ettus USRP B205mini;
- Great Scott Gadgets HackRF One; and
- Nuand bladeRF 2.0 micro xA9.

The 902–928 MHz industrial, scientific, and medical (ISM) band provides a common measurement region for all five receivers. The 2402–2480 MHz range, which spans the Bluetooth channel centers, provides a second region for the receivers that support it, allowing comparison across widely separated frequencies in an environment with substantial wireless activity (Bluetooth Special Interest Group, n.d.).

The receivers differ in tuning range, sampling capability, and practical passband behavior. The RTL-SDR V3 and SMArt XTR provide lower-rate configurations (RTL-SDR Blog, n.d.; Nooelec, 2022), whereas the B205mini, HackRF One, and bladeRF support the 10 MS/s profiles used here (Ettus Research, n.d.a; Great Scott Gadgets, n.d.a; Nuand, n.d.). HackRF documentation recommends against sampling below 8 MS/s because of analog-to-digital converter and baseband-filter limitations (Great Scott Gadgets, n.d.b). These specifications, shown along

Proceedings of the 16th GNU Radio Conference,

with other device information in Table 1, together with the behavior observed in the processing chain, informed the selection of participating receivers in Table 2.

Prior work has demonstrated FFT-based spectrum sensing with GNU Radio and USRP hardware (Rashid et al., 2011), compared energy- and autocorrelation-based scanning techniques (Subramaniam et al., 2015), and proposed common procedures for experimental evaluation of signal detectors (Šolc et al., 2018). Building on this work, the present study evaluates five commercially available SDRs as practical platforms for calibrated spectrum sensing and detection. Using a common sequential energy detector and consistent scan geometry within each parameter profile, the evaluation compares the empirical false-alarm behavior, repeatability, and scan time of the receivers.

The comparison uses per-subband timing measurements and terminated-input false-alarm measurements, supplemented by controlled-signal checks and illustrative over-the-air scans. Two sampling configurations are considered: 2.4 MS/s with a center-frequency spacing of $\Delta f = 2$ MHz, and 10 MS/s with $\Delta f = 5$ MHz. Receiver-specific settling intervals are used to assess scan speed under configurations that supported reliable detection in the controlled tests.

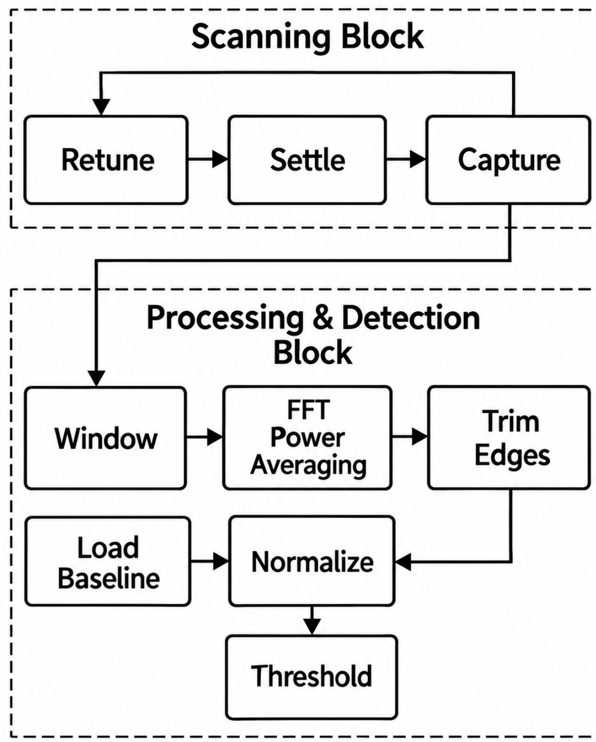

Figure 1. Sequential acquisition and detection pipeline.

2. Methods

2.1. Sequential Scanning

The system uses GNU Radio embedded Python blocks to acquire in-phase and quadrature (IQ) samples by sequentially tuning across a prescribed frequency range. Adjacent center frequencies are separated by Δf. With f_{start} and f_{stop} denoting the lower and upper limits of the center-frequency sequence, the number of centers is

$$K = \left\lfloor \frac{f_{\text{stop}} - f_{\text{start}}}{\Delta f} \right\rfloor + 1. \tag{1}$$

The final center may therefore lie below f_{stop} when the interval is not an integer multiple of Δf. Sampling at $f_s > \Delta f$ permits removal of edge bins before stitching. With this structure, the full covered range is 901-929 MHz for the 2.4 MS/s profile and 899.5-929.5 MHz and 2399.5-2479.5 MHz for the 10 MS/s profile. The scanner records a fixed number of samples, issues a retune command, and discards samples over a settling interval before recording at the next center frequency. This interval allows the receiver to complete tuning and reduces contamination by samples associated with the previous center frequency. Figure 1 summarizes acquisition and processing. Timing comparisons use the smallest settling interval found to support reliable detection for each receiver in the controlled tests, as reported in Table 3.

2.2. Frequency Response Normalization

After each subband capture, the samples are passed to a processing and detection block while the scanner proceeds to the next subband. The IQ data are divided into M consecutive, nonoverlapping frames of N samples, each multiplied by a Blackman window. An N-point FFT is computed for each frame, and the squared magnitudes are averaged to obtain the subband power spectrum. Averaging modified periodograms reduces the variability of the spectral estimate (Bartlett, 1948; Welch, 1967), while the window controls spectral leakage (Harris, 1978).

A noise-only baseline is recorded with the receiver input terminated in 50 Ω load, using a substantially larger number of frames than in an individual detection batch. Dividing the measured power by this baseline compensates for the receiver's frequency-dependent noise response. The overlapping capture bandwidths permit removal of edge bins affected by analog-filter roll-off before the retained spectra are stitched. For FFT length N, the number of bins removed from each edge is

$$C = \left\lceil \frac{(f_s - \Delta f)N}{2 f_s} \right\rceil . \tag{2}$$

The remaining $N - 2C$ bins from successive centers are

Table 1. Device specifications. SMArt XTR reports a gap in its tuning range at 1100 MHz.

Receiver	Price	Tuning Range	Max f_s	ADC bits	Host Interface
RTL-SDR V3	\$35	0.5-1766 MHz	2.4 MS/s	8-bit	USB 2.0
SMArt XTR	\$55	55-2300 MHz	2.4 MS/s	8-bit	USB 2.0
B205mini	\$1875	70-6000 MHz	61.44 MS/s	12-bit	USB 2.0
HackRF One	\$340	1-6000 MHz	20 MS/s	8-bit	USB 2.0
bladeRF xA9	\$860	47-6000 MHz	61.44 MS/s	12-bit	USB 2.0

Table 2. Frequency-range and sampling profiles.

Center-frequency range	f_s	Δf	Participating SDRs
902–928 MHz	2.4 MS/s	2 MHz	B205mini, RTL-SDR V3, SMArt XTR
902–928 MHz	10 MS/s	5 MHz	B205mini, HackRF One, bladeRF xA9
2402–2480 MHz	10 MS/s	5 MHz	B205mini, HackRF One, bladeRF xA9

concatenated in ascending frequency. This normalization provides a relative measure with respect to the terminated-input baseline.

2.3. Energy Detection

The system uses a threshold-based energy detector. For each subband, it averages M FFT frames of length N, where $M = \lfloor f_s T_d / N \rfloor$ and T_d is the subband dwell time in seconds. The experiments use $N = 1024$. Let $x_m[n]$, $n = 0, \dots, N-1$, denote the mth frame. Its windowed N-point DFT is

$$Y_m[k] = \sum_{n=0}^{N-1} w[n] x_m[n] e^{-j2\pi kn/N}, \tag{3}$$

where $w[n]$ is the Blackman window. The FFT bins are subsequently shifted for frequency-ordered display and stitching. At a given bin, the detection problem is expressed as

$$\mathcal{H}_0 : Y_m[k] = W_m[k], \tag{4}$$

$$\mathcal{H}_1 : Y_m[k] = S_m[k] + W_m[k], \tag{5}$$

where $W_m[k]$ and $S_m[k]$ denote the noise and signal contributions, respectively.

Averaging the squared magnitudes over M frames gives the per-bin energy statistic

$$T[k] = \frac{1}{M} \sum_{m=0}^{M-1} |Y_m[k]|^2. \tag{6}$$

The terminated-input baseline gives a finite-sample estimate $\widehat{\mu}_0[k]$ of the true mean noise power $\mu_0[k]$. The implemented normalized statistic and its ideal known-mean counterpart are defined respectively as

$$\begin{aligned} R[k] &= \frac{T[k]}{\widehat{\mu}_0[k]}, \\ R_0[k] &= \frac{T[k]}{\mu_0[k]}. \end{aligned} \tag{7}$$

For zero-mean, proper complex Gaussian noise that is independent across frames, the ideal noise-only distribution is

$$2MR_0[k] \sim \chi^2_{2M} \qquad \text{under } \mathcal{H}_0. \tag{8}$$

This is the complex-sample form of the classical energy-detection model (Urkowitz, 1967). The per-bin false-alarm probability is

$$\begin{aligned} P_{\mathrm{FA,bin}} &= \Pr(R_0[k] > \eta_M \mid \mathcal{H}_0) \\ &= 1 - F_{\chi^2_{2M}}(2M\eta_M)\,. \end{aligned} \tag{9}$$

Solving for the normalized threshold with the chi-square quantile function $F^{-1}_{\chi^2_{2M}}$ and the indicator function $\mathbf{1}\{\cdot\}$ gives

$$\eta_M = \frac{F^{-1}_{\chi^2_{2M}}(1 - P_{\mathrm{FA,bin}})}{2M}, \tag{10}$$

and the final per-bin detection decision is

$$\widehat{D}[k] = \mathbf{1}\{R[k] > \eta_M\}. \tag{11}$$

Because the implemented baseline is estimated from a finite capture, the exact distribution is for the normalized statistic is given by an F distribution with $(2M, 2M_b)$ degrees of freedom.

$$R[k] \sim F_{2M,\,2M_b}, \tag{12}$$

where M_b is the number of averaged baseline frames. Given that $M_b >> M$, the chi-square limit is appropriate.

For $N - 2C$ retained bins, the ideal expected number of false detections per subband is

$$\mathbb{E}[N_{\mathrm{FA}}] = (N - 2C) P_{\mathrm{FA,bin}}. \tag{13}$$

The empirical mean count, $\overline{N}_{\mathrm{FA}}$, is measured using terminated-input captures and compared with this expectation to assess receiver repeatability. The expectation in (13) does not require independence between bins, although bin dependence affects the variability of the count and the probability of at least one false detection.

2.4. Experiment Setup

The receivers were evaluated using the frequency ranges and sampling rates in Table 2. The 2.4 MS/s configuration was selected for the lower-rate receivers, while 10 MS/s was the largest rate found to operate reliably with the processing chain used in these experiments. These are experimental operating points, rather than universal device limits. The calibration baseline averaged 1 second of data for each subband, resulting in 2343 and 9765 averaged frames for the 2.4 MS/s and 10 MS/s profiles.

All SDRs were connected via USB 2.0 to a Intel(R) Core(TM) Ultra 7 155H (1.40 GHz) CPU with. The experiments were run with GNU Radio 3.10.12.0 on a Windows 11, 64-bit Operating System. The RX gain was set and kept fixed for each receiver at 15 dB for the RTL-SDR V3, SMArt XTR, and bladeRF xA9, and 30 dB for the B205mini. The HackRF distributes gain directly between IF and VGA. Both were set to a value of 16 dB. AGC was disabled for the receivers that support it. These values reflect device specific settings exposed to GNU Radio and are not comparable between SDRs. Each profile used a proxicast ant-120-008 semi-wideband antenna in an indoor lab environment to maintain a consistent comparison.

Evaluation focuses on timing statistics and empirical false-alarm counts. Controlled over-the-air signals were used to check detector operation and settling behavior at the selected per-bin false-alarm probability of $P_{\mathrm{FA,bin}} = 10^{-5}$. A quantitative signal-level detection probability is not reported because a rule for converting the per-bin mask into individual signal decisions has not been defined. Instead, terminated-input, noise-only captures in the 902–928 MHz band assess false detections and consistency with the baseline. Figures 2 and 3 illustrate the normalized power spectra and detection masks for over-the-air scans.

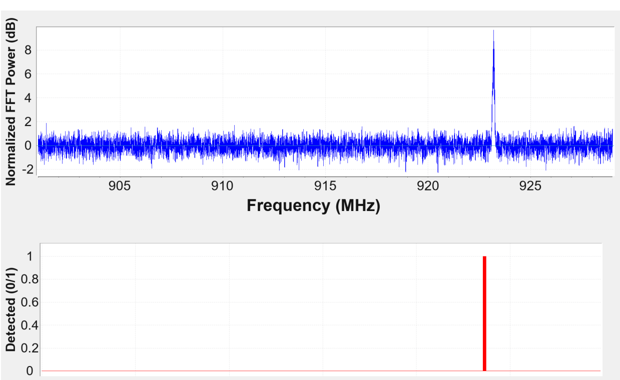

Figure 2. Normalized power spectrum (top) and per-bin detection mask (bottom) for a B205mini scan in the 902–928 MHz ISM band at 2.4 MS/s.

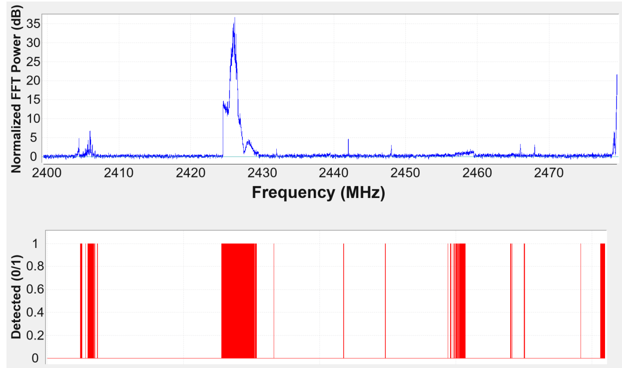

Figure 3. Normalized power spectrum and per-bin detection mask for a B205mini scan across the 2.4 GHz monitoring range at 10 MS/s.

3. Results

3.1. Settling Interval

The settling interval was varied in 5 ms increments to identify the smallest tested value that supported reliable detection in every subband. Signals with known center frequencies and bandwidths were used to check for contamination from the preceding tuning state. Table 3 reports the resulting intervals. These values characterize the tested receiver configurations.

Table 3. Smallest tested settling interval T_{settle} supporting a stable receiver response and no contamination from the previous center.

Receiver	T_{settle}
RTL-SDR V3	0 ms
SMArt XTR	30 ms
B205mini	30 ms
HackRF One	25 ms
bladeRF xA9	15 ms

3.2. Timing Performance

Table 4 compares the receiver profiles at a dwell time of $T_d = 30$ ms, with statistics averaged over 50 trials. T_{total} denotes the reported time from flowgraph startup to shutdown for a complete scan. T_{scan} is the mean interval from the retune command to the end of capture for a subband, and T_{detect} is the mean time to process that subband and compute its detection mask.

The mean processing time is below the 30 ms dwell time for every tested profile, indicating average processing headroom for acquisition and detection to proceed concurrently. The per-subband scan interval also exceeds the dwell time in every profile. This difference includes settling, retuning, and data-delivery overhead. Acquiring multiple de-

Table 4. Mean and standard-deviation timing results over 50 trials with $T_d = 30$ ms.

Receiver	Frequency range	f_s	$\overline{T}_{\text{total}}$	$\overline{T}_{\text{scan}}$	σ_{scan}	$\overline{T}_{\text{detect}}$	σ_{detect}
RTL-SDR V3	902–928 MHz	2.4 MS/s	0.707 s	45.29 ms	1.96 ms	8.27 ms	0.81 ms
SMArt XTR	902–928 MHz	2.4 MS/s	1.091 s	72.72 ms	3.07 ms	8.15 ms	0.86 ms
B205mini	902–928 MHz	2.4 MS/s	1.038 s	73.49 ms	0.85 ms	11.87 ms	0.90 ms
HackRF One	902–928 MHz	10 MS/s	0.480 s	77.44 ms	3.88 ms	16.31 ms	1.74 ms
bladeRF xA9	902–928 MHz	10 MS/s	0.522 s	82.71 ms	8.11 ms	16.87 ms	3.30 ms
B205mini	902–928 MHz	10 MS/s	0.931 s	153.85 ms	11.32 ms	17.08 ms	1.44 ms
HackRF One	2402–2480 MHz	10 MS/s	1.344 s	82.96 ms	5.11 ms	16.50 ms	2.26 ms
bladeRF xA9	2402–2480 MHz	10 MS/s	1.570 s	96.47 ms	5.34 ms	17.16 ms	1.92 ms
B205mini	2402–2480 MHz	10 MS/s	2.223 s	138.38 ms	7.24 ms	18.26 ms	1.99 ms

tection batches at each center frequency could reduce the average retuning overhead per batch, allowing proportionately more time for spectrum monitoring, at the expense of longer revisit intervals for other subbands.

3.3. Detection Performance and Repeatability

The nominal setting $P_{\text{FA,bin}} = 10^{-5}$ was used throughout the reported false-alarm comparison. Figure 4 shows the mean number of false detections per subband as a function of center frequency for the B205mini, RTL-SDR V3, and bladeRF. The largest deviations are localized in frequency and are consistent with receiver-dependent spurious components.The receiver response during a 30 ms detection batch can differ from the response captured by the calibration baseline, which averages approximately 10^7 samples.

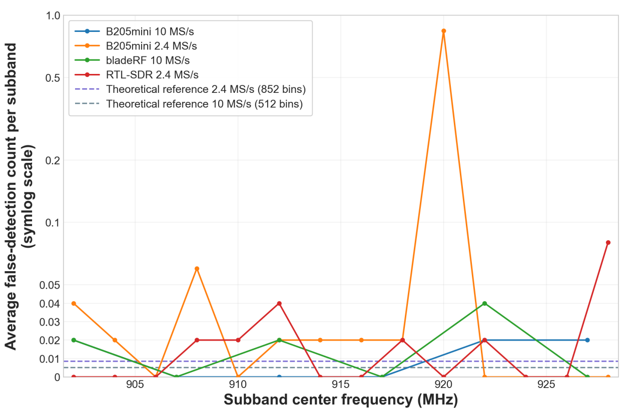

Figure 4. Mean false-detection count per subband over 50 noise-only trials in the 902–928 MHz band. The HackRF One and SMArt XTR are omitted to show variation among the lower-count configurations. Dashed lines indicate the theoretical expected counts.

Table 5 compares empirical mean false-detection counts per subband with the ideal expectation in (13). With $N = 1024$, the two profiles retain 852 and 512 bins, giving expected counts of 0.00852 and 0.00512, respectively. The 50 trials provide a descriptive comparison of practical performance rather than a rigorous validation of the theoretical expectation.

Figure 5 illustrates the elevated false detections observed with the HackRF One in a noise-only capture. Narrowband spurious components can differ between the detection batch and the calibration baseline, producing threshold crossings after normalization.

Under the tested configurations, the B205mini, RTL-SDR V3, and bladeRF have reasonable mean false-detection counts, approximately 2x above the theoretical expectation. This consistent factor is likely caused by a combination of finite-baseline estimation bias, residual spurs, or inter-bin correlation from the Blackman window.

The HackRF One and SMArt XTR both reported orders of magnitude higher false-detection counts than their expected mean, indicating that baseline-normalization fails for these two receivers under these configurations. This is attributed to stochastic receiver artifacts with high variation from their mean value as approximated by the finite-sample baseline.

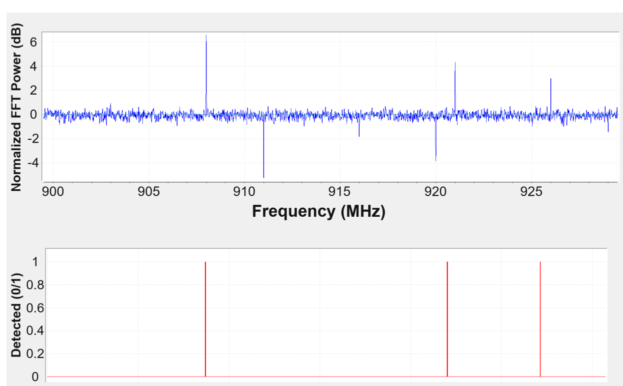

Figure 5. Normalized power spectrum with respect to and detection mask for a noise-only HackRF One capture. Narrowband receiver artifacts produce false detections despite baseline normalization.

The aggregate activity illustrated in the 2.4 GHz scan in Figure 3 motivates shorter integration intervals for observ-

Table 5. Mean false-detection counts per subband in the 902–928 MHz band over 50 trials at each dwell time. 6 subband centers for the 2.4 MS/s profile and 14 for the 10 MS/s profile give 300 and 700 subband trials respectively. The ideal expectation uses $P_{\mathrm{FA,bin}} = 10^{-5}$.

Receiver	f_s	$\mathbb{E}[N_{\mathrm{FA}}]$	$\overline{N}_{\mathrm{FA}}$, 30 ms	$\overline{N}_{\mathrm{FA}}$, 10 ms
RTL-SDR V3	2.4 MS/s	0.00852	0.0143	0.0143
SMArt XTR	2.4 MS/s	0.00852	6.7586	2.3329
B205mini	2.4 MS/s	0.00852	0.0743	0.0143
B205mini	10 MS/s	0.00512	0.0100	0.0100
HackRF One	10 MS/s	0.00512	1.9000	2.3100
bladeRF xA9	10 MS/s	0.00512	0.0133	0.0233

ing intermittent transmissions. Reducing the dwell time to $T_d = 10$ ms provides a shorter integration interval. Table 5 shows that the effect on false detections is receiver dependent: the mean count decreases for the SMArt XTR and the B205mini at 2.4 MS/s, remains unchanged for the RTL-SDR V3 and the B205mini at 10 MS/s, and increases for the HackRF One and bladeRF. At this dwell time, the reported mean processing times lie between 4 and 7 ms, with few batches exceeding 10 ms. These results show sufficient average processing throughput for continuous acquisition and concurrent detection of 10 ms frames within a fixed subband.

Figure 4 also shows sensitivity to the sampling configuration within a single receiver. At 2.4 MS/s, the B205mini exhibits an elevated mean false-detection count near the 920 MHz scan center. Analysis of the underlying per-bin detection masks showed that this elevated count was concentrated in three adjacent bins near 920 MHz, where the calibration baseline also contained a narrowband artifact. The same localized excess is absent from the 10 MS/s results. This comparison suggests that baseline consistency depends on the receiver's operating configuration as well as its model. It also illustrates how a small number of predictably problematic bins can disproportionately influence the reported false-detection count.

3.4. Qualitative Observations

The timing and false-alarm measurements also reveal practical differences among the tested receivers.

RTL-SDR V3. This low-cost receiver was the only device that supported reliable detection without any post-retune settling interval. Within the tested frequency range, it produced low and consistent false-detection counts without any localization in frequency.

Nooelec NESDR SMArt XTR. The SMArt XTR produced the highest mean false-detection count in Table 5. Spectral inspection indicated that many of these detections were concentrated around variable receiver artifacts rather than distributed uniformly across the band.

Ettus USRP B205mini. The B205mini supported both sampling rates and both frequency ranges, although its 10 MS/s scan times exceeded those of the other receivers in the same profiles. The implementation used local-oscillator offset tuning, supported by the UHD tuning interface, to place the associated DC offset outside the retained passband (Ettus Research, n.d.b).

Great Scott Gadgets HackRF One. The HackRF One provided the shortest mean full-scan times in both 10 MS/s profiles, but with elevated false detections in the terminated-input tests. The tested implementation also required additional settling for the first subband after startup. This startup-specific interval was excluded from the per-subband timing statistics.

Nuand bladeRF 2.0 micro xA9. The bladeRF required the shortest post-retune settling interval among the three receivers in the 10 MS/s profiles and produced low mean false-detection counts. In the tested configurations, passband-edge behavior motivated oversampling and discarding edge bins before stitching.

4. Conclusion

This paper compares five commercial SDRs for calibrated spectrum sensing using a common sequential energy detector. The results characterize scan time, terminated-input false detections, and repeatability across the tested receiver configurations. Within their respective profiles the B205mini, bladeRF, and RTL-SDR V3 produced lower mean false-detection counts than the HackRF One and SMArt XTR. The HackRF One completed scans faster than its peers in both 10 MS/s profiles, with elevated false detections associated with receiver artifacts. The SMArt XTR had the longest full-scan time in the 2.4 MS/s profile and the highest mean false-detection count.

The timing analysis shows that per-subband acquisition includes appreciable overhead beyond the 30 ms dwell time. Collecting several detection batches before retuning could amortize the retuning and settling overhead over several batches, increasing the fraction of scan time spent acquiring. The resulting tradeoff between time spent at one center frequency and revisits to the remaining band should be considered when selecting a scan strategy.

Shorter integration intervals may provide more informative observations of intermittent activity in the 2.4 GHz range. The reported processing times support the practicality of 10 ms detection batches in the tested configurations. Shortening the dwell time did not systematically increase false detections attributable to background noise. Instead, changes in the total counts primarily reflected how the amplitudes of receiver-generated harmonics in each short detection batch differed from their levels in the calibration baseline, which was averaged over approximately 10^7 samples. FFT length, dwell time, and sampling rate can therefore be selected according to the spectral and temporal requirements of the monitoring task.

Further work should develop a signal-level decision rule that groups adjacent detected bins into candidate signals and rejects isolated false detections while retaining sensitivity to sparsely detected, low SNR signals and narrowband tones. Such a rule would support downstream applications, including dynamic spectrum access and automatic modulation classification. The observed concentration of false detections in specific frequency regions also motivates investigating masks or reduced decision weights for persistent receiver artifacts. Any such approach should assess the resulting loss of sensitivity to signals occupying those regions. Additionally, more rigorous treatment of per-bin detection relative to SNR would add to the understanding of these SDRs' reliability at the configured false-detection rate.

References

Bartlett, M. S. Smoothing periodograms from time-series with continuous spectra. *Nature*, 161(4096):686–687, 1948. doi: 10.1038/161686a0.

Bluetooth Special Interest Group. Bluetooth core specification, version 6.2: Radio physical layer specification. https://www.bluetooth.com/wp-content/uploads/Files/Specification/HTML/Core-62/out/en/low-energy-controller/radio-physical-layer-specification.html, n.d. Vol. 6, Part A, Sec. 2; accessed 2026-09-13.

Chiper, Florin-Lucian, Martian, Alexandru, Vladeanu, Calin, Marghescu, Ion, Craciunescu, Razvan, and Fratu, Octavian. Drone detection and defense systems: Survey and a software-defined radio-based solution. *Sensors*, 22(4):1453, 2022. doi: 10.3390/s22041453.

Ettus Research. UHD and USRP manual: USRP B2x0 series. https://files.ettus.com/manual/page_usrp_b200.html, n.d.a. Accessed 2026-09-13.

Ettus Research. UHD and USRP manual: General application notes. https://files.ettus.com/manual/page_general.html, n.d.b. Tuning notes; accessed 2026-09-13.

Great Scott Gadgets. HackRF One. https://hackrf.readthedocs.io/en/stable/hackrf_one.html, n.d.a. Product documentation; accessed 2026-09-13.

Great Scott Gadgets. Sampling rate and baseband filters. https://hackrf.readthedocs.io/en/stable/sampling_rate.html, n.d.b. HackRF documentation; accessed 2026-09-13.

Harris, Fredric J. On the use of windows for harmonic analysis with the discrete fourier transform. *Proceedings of the IEEE*, 66(1):51–83, 1978. doi: 10.1109/PROC.1978.10837.

Khan, Muhammad Asif, Menouar, Hamid, Eldeeb, Aisha, Abu-Dayya, Adnan, and Salim, Flora D. On the detection of unauthorized drones—techniques and future perspectives: A review. *IEEE Sensors Journal*, 22(12):11439–11455, 2022. doi: 10.1109/JSEN.2022.3171293.

Mariani, Andrea, Giorgetti, Andrea, and Chiani, Marco. Effects of noise power estimation on energy detection for cognitive radio applications. *IEEE Transactions on Communications*, 59(12):3410–3420, 2011. doi: 10.1109/TCOMM.2011.102011.100708.

Nooelec. NESDR series. https://support.nooelec.com/hc/en-us/articles/360005805834-NESDR-Series, 2022. Updated November 24, 2022; accessed 2026-09-13.

Nuand. bladeRF 2.0 micro. https://www.nuand.com/bladerf-2-0-micro/, n.d. Product specifications; accessed 2026-09-13.

Rashid, Rozeha A., Sarijari, Mohd Adib, Fisal, Norsheila, Lo, Anthony, Yusof, Sh. Kamilah S., and Mahalin, Nurhija. Spectrum sensing measurement using GNU Radio and USRP software radio platform. In *ICWMC 2011, The Seventh International Conference on Wireless and Mobile Communications*, pp. 237–242. IARIA, 2011. URL https://www.thinkmind.org/articles/icwmc_2011_11_20_20268.pdf.

RTL-SDR Blog. RTL-SDR Blog V3 datasheet. https://www.rtl-sdr.com/wp-content/uploads/2018/02/RTL-SDR-Blog-V3-Datasheet.pdf, n.d. Accessed 2026-09-13.

Šolc, Tomaž, Mohorčič, Mihael, and Fortuna, Carolina. A methodology for experimental evaluation of signal detection methods in spectrum sensing. *PLOS ONE*, 13(6):e0199550, 2018. doi: 10.1371/journal.pone.0199550.

Subramaniam, Sriram, Reyes, Hector, and Kaabouch, Naima. Spectrum occupancy measurement: An autocorrelation based scanning technique using USRP. In *2015 IEEE 16th Annual Wireless and Microwave Technology Conference (WAMICON)*, pp. 1–5, 2015. doi: 10.1109/WAMICON.2015.7120376.

Tandra, Rahul and Sahai, Anant. SNR walls for signal detection. *IEEE Journal of Selected Topics in Signal Processing*, 2(1):4–17, 2008. doi: 10.1109/JSTSP.2007.914879.

Urkowitz, Harry. Energy detection of unknown deterministic signals. *Proceedings of the IEEE*, 55(4):523–531, 1967. doi: 10.1109/PROC.1967.5573.

Welch, Peter D. The use of fast fourier transform for the estimation of power spectra: A method based on time averaging over short, modified periodograms. *IEEE Transactions on Audio and Electroacoustics*, 15(2):70–73, 1967. doi: 10.1109/TAU.1967.1161901.

Yücek, Tevfik and Arslan, Hüseyin. A survey of spectrum sensing algorithms for cognitive radio applications. *IEEE Communications Surveys & Tutorials*, 11(1):116–130, 2009. doi: 10.1109/SURV.2009.090109.